Electronic Supplementary Material (ESI) for Nanoscale Advances.

Supporting Information: Determining the morphology and concentration of core-shell Au/Ag nanoparticles

Jieli Lyu,[†] Valérie Geertsen,[‡] Cyrille Hamon,[*,†] and Doru Constantin[*,†]

†*Université Paris-Saclay, CNRS, Laboratoire de Physique des Solides, 91405 Orsay, France.*

‡*Université Paris-Saclay, CEA, CNRS, NIMBE, 91190 Gif-sur-Yvette, France.*

E-mail: cyrille.hamon@u-psud.fr; doru.constantin@u-psud.fr

Transmission electron microscopy

Figure S1 shows the histograms of particle radius distributions obtained by TEM as well as the associated means and standard deviations. Figures S2 through S10 show TEM images for $K = 0$ through 8.

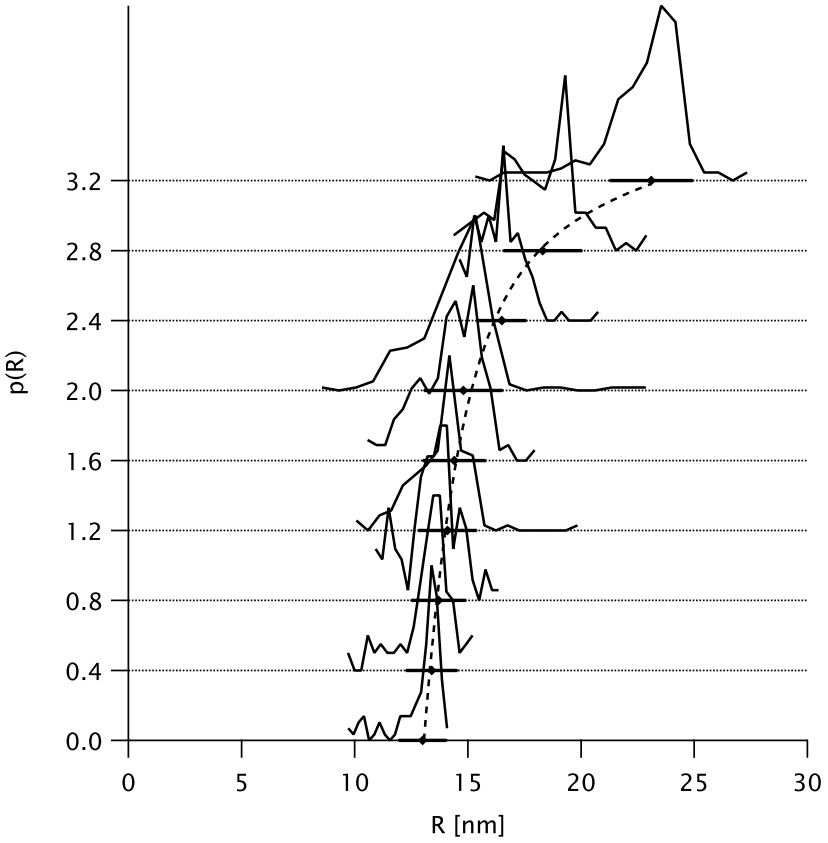

Figure S1: Particle radius histograms extracted from the TEM images. The mean and standard deviation are shown as diamonds and bars. For clarity, the curves are shifted upwards in steps of 0.4. The dashed line is a guide to the eye. The molar Ag/Au ratios K are (from bottom to top): 0, 0.4, 0.7, 0.9, 1.2, 1.4, 2, 4, and 8.

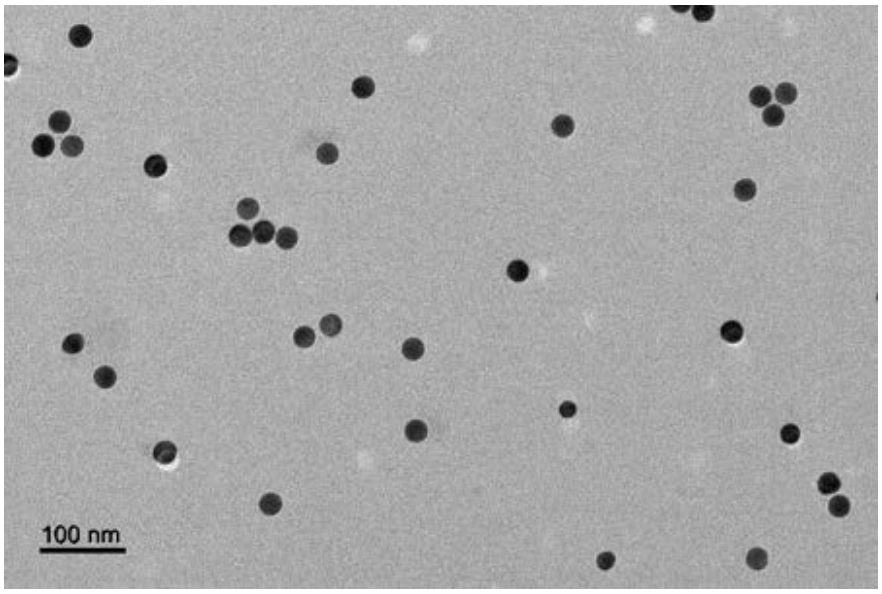

Figure S2: TEM image for $K = 0$.

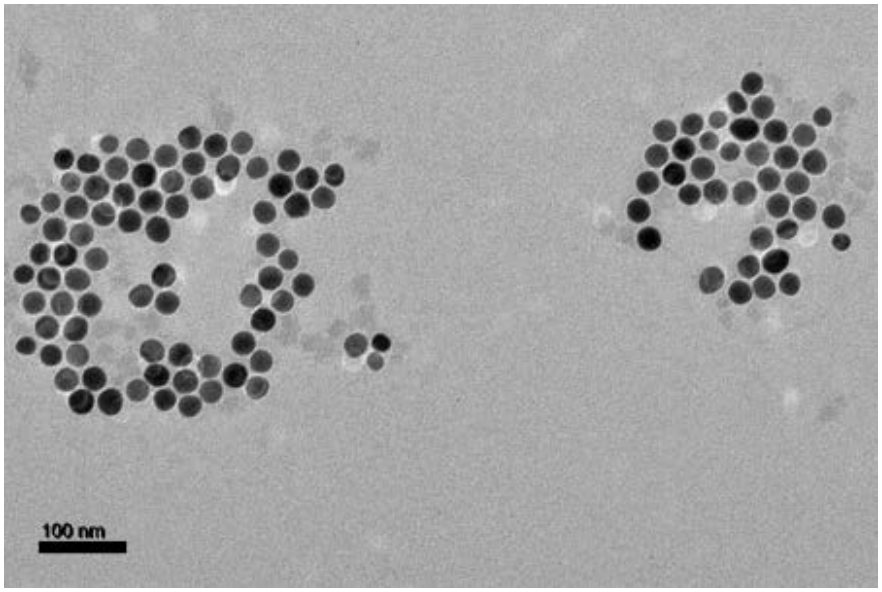

Figure S3: TEM image for $K = 0.4$.

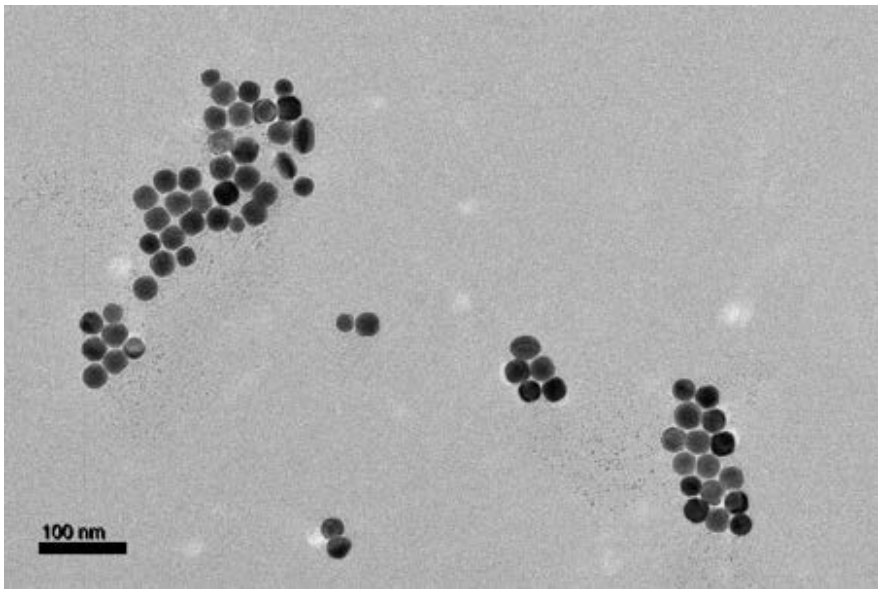

Figure S4: TEM image for $K = 0.7$.

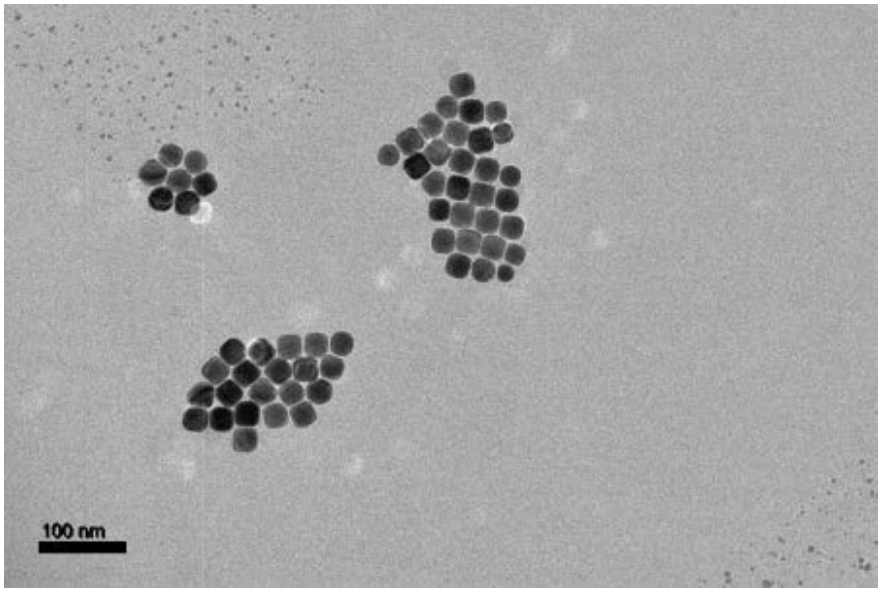

Figure S5: TEM image for $K = 0.9$.

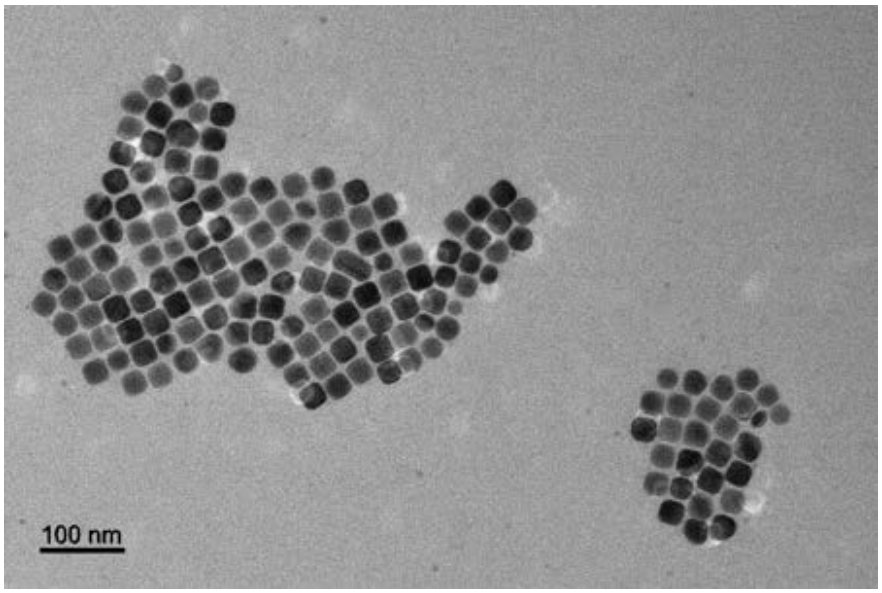

Figure S6: TEM image for $K = 1.2$.

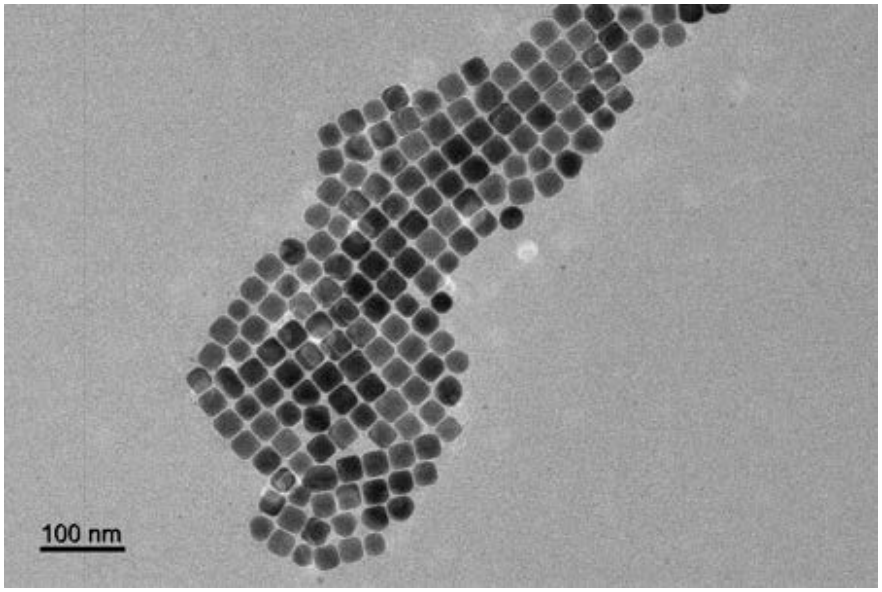

Figure S7: TEM image for $K = 1.4$.

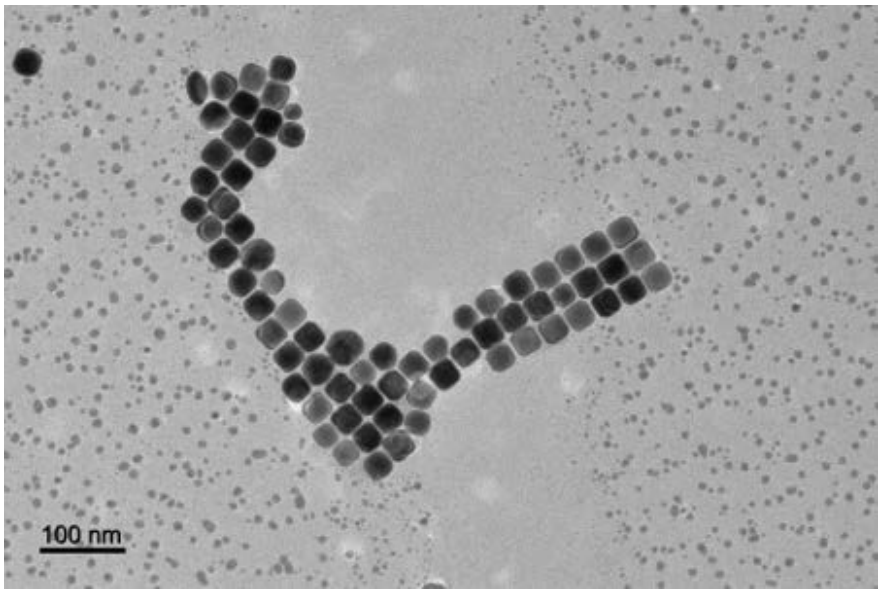

Figure S8: TEM image for $K = 2.0$.

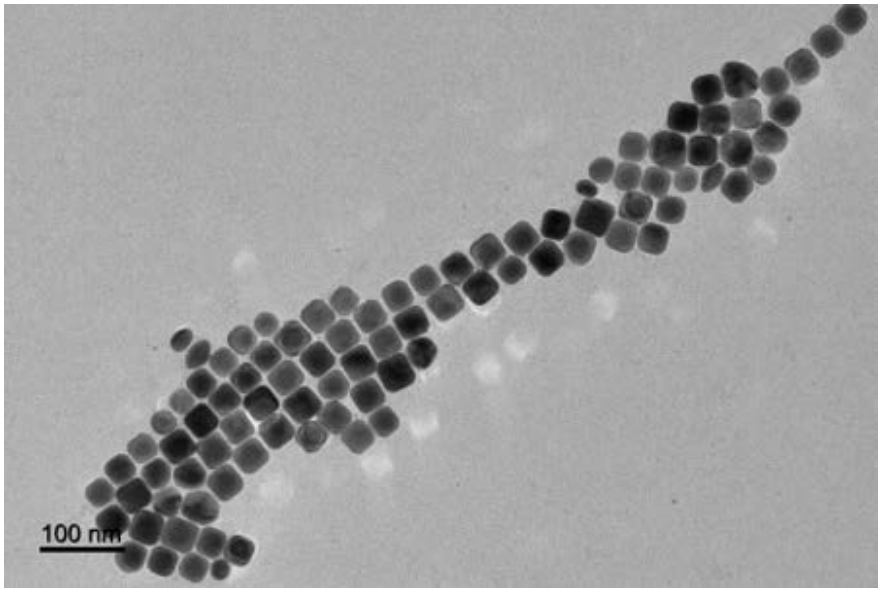

Figure S9: TEM image for $K = 4.0$.

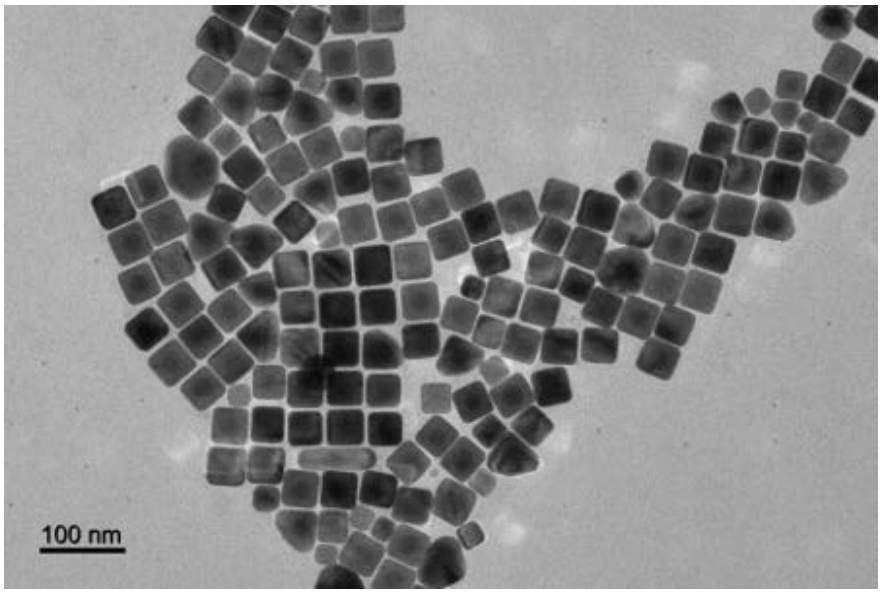

Figure S10: TEM image for $K = 8.0$.

SAXS form factor

The scattering signal I of a dilute colloidal solution as a function of the scattering vector q can be written as:

$$I(q) = \frac{scale}{V_{\text{tot}}} \left\langle |G|^2 \right\rangle_{\theta,\varphi} + bkg \tag{1}$$

where *scale* is a scale factor proportional to the volume fraction of the objects in solution, V_{tot} is the total volume of the particle, bkg is a residual background term, G is the (anisotropic) form factor of the particle (defined below) averaged over the polar and azimuthal angles θ and φ, respectively.

Depending on the shape of the shell (sphere or cube), the composite objects are modeled as either:

1. gold spheres with radius R, contained within silver spherical shells with outer radius $R + t$, see Figure S11a).

2. or gold spheres with radius R, contained within silver cubic shells of side length a, see Figure S11b).

In both cases we assume that the spheres are centered within the shells, based on the TEM images.

Sphere in sphere

In this case, we use the PolyCoreShellRatio function available in the NCNR SANS package,[S1] implementing a core-shell spherical model with a homothetical polydispersity described by the Schulz model.

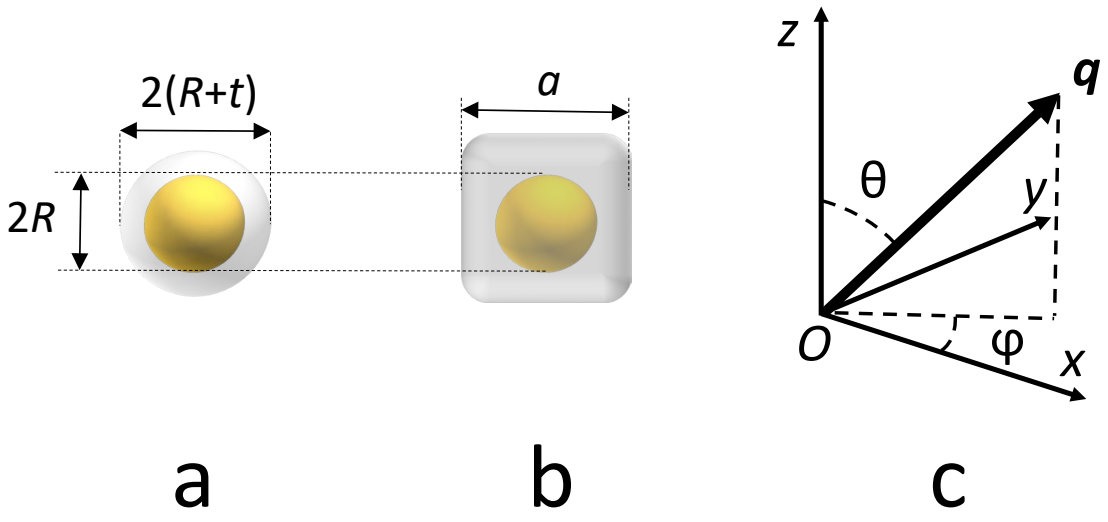

Figure S11: Diagram of the a) sphere in sphere and b) sphere in cube. c) Scattering geometry.

Sphere in cube

The form factor in (1) is:

$$G = c_1 f_1 + c_2 f_2 = \tag{2}$$
$$\Delta\rho_{\mathrm{sm}}\, a^3\, f_1(a, q, \theta, \varphi) + \Delta\rho_{\mathrm{cs}}\, 4\pi R^3\, f_2(R, q).$$

On the right-hand side of the equation, we expanded the c_i constants in terms of the particle sizes defined above and the scattering length density (SLD) contrast between shell (silver) and the surrounding medium (water) $\Delta\rho_{\mathrm{sm}} = \rho_{\mathrm{s}} - \rho_{\mathrm{m}}$ and between core (gold) and shell, $\Delta\rho_{\mathrm{cs}} = \rho_{\mathrm{c}} - \rho_{\mathrm{s}}$. The individual form factors f_i depend on the particle dimensions (a and R) and on the scattering geometry (absolute value q and orientation angles θ and φ of the scattering vector $\mathbf{q}$ with respect to the particle reference system, see Figure S11c).

$$f_1(a, q, \theta, \varphi) = \mathrm{sinc}\left(\frac{qa}{2}\sin\theta\cos\varphi\right)\mathrm{sinc}\left(\frac{qa}{2}\sin\theta\sin\varphi\right)\mathrm{sinc}\left(\frac{qa}{2}\cos\theta\right) \tag{3}$$
$$f_2(R, q) = \frac{\sin(qR) - qR\cos(qR)}{(qR)^3}$$

The angular integration $\langle\cdot\rangle_{\theta,\varphi} = \int_0^{\pi} \sin\theta \, \mathrm{d}\theta \int_0^{2\pi} \mathrm{d}\varphi \cdot$ is done using the Integrate2D operation in Igor Pro 7.0.

Polydispersity

In the sphere-in-cube model, we account for the polydispersity by introducing a homothetical size distribution: both dimensions are scaled by a parameter λ with respect to their reference values R_0 and a_0 (in which case the scattered signal is $I_0(q)$, corresponding to $\lambda = 1$) and λ is distributed along a Gaussian:

$$d(\lambda) = \frac{1}{\sqrt{2\pi}p} \exp\left[-\frac{1}{2}\left(\frac{\lambda - 1}{p}\right)^2\right] \tag{4}$$

Scaling all sizes by λ or the scattering vector q by the same factor preserves the signal, up to a λ^6 prefactor (easily understood if we recall that the scattered intensity is proportional to the particle volume squared.) The polydisperse signal can then be obtained as:

$$I_{\mathrm{avg}}(q) = \int \mathrm{d}\lambda \, \lambda^6 d(\lambda) I_0(\lambda q) \tag{5}$$

Absorbance spectroscopy model

We model the objects as core-shell spherical objects, with inner radius R_1 and outer radius R_2, core volume $V_1 = (4\pi/3)R_1^3$ and total volume $V = (4\pi/3)R_2^3$. The core volume fraction $f = V_1/V$. The dielectric constant of the medium (water, in our case) is ϵ_m, that of the core (gold) is $\epsilon(\lambda)$ and that of the shell (silver) $\epsilon_s(\lambda)$. The latter values are taken from S2 and size-corrected as detailed in S3.

In the Rayleigh (or quasistatic) regime, the polarizability of homogeneous and core-shell spherical particles is well-known:[S4] $P(\lambda) = 3V\epsilon_m\alpha(\lambda)$, with:

$$\alpha_{\mathrm{H}}(\lambda) = \frac{\epsilon - \epsilon_m}{\epsilon + 2\epsilon_m} \tag{6}$$

for a homogeneous sphere and

$$\alpha_{\mathrm{CS}}(\lambda) = \frac{(2\epsilon_s + \epsilon)(\epsilon_s - \epsilon_m) + f(\epsilon - \epsilon_s)(2\epsilon_s + \epsilon_m)}{(2\epsilon_s + \epsilon)(\epsilon_s + 2\epsilon_m) + 2f(\epsilon - \epsilon_s)(\epsilon_s - \epsilon_m)} = \frac{\alpha_2 - f\dfrac{\alpha_1\alpha_2}{\alpha_3}}{1 + 2f\alpha_1\alpha_2} \tag{7}$$

for a core-shell particle. The wavelength dependence of $\alpha(\lambda)$ is due to that of $\epsilon(\lambda)$ and $\epsilon_s(\lambda)$. For simplicity, we do not indicate the argument explicitly in (7). In the second expression above, the α_j are the following homogeneous polarizabilities, defined as in (6): α_1 – sphere with dielectric constant ϵ in a medium with dielectric constant ϵ_s; α_2 – ϵ_s in ϵ_m; α_3 – ϵ_m in ϵ_s.

For larger particle sizes, the deviation from the Rayleigh regime is accounted for in the long-wavelength approximation (LWA),[S5] as applied to a core-shell object by Chung et al.,[S6,S7] rewritten below in terms of the homogeneous polarizabilities α_j:

$$\alpha(\lambda) = \frac{\alpha_2 - f\dfrac{\alpha_1\alpha_2}{\alpha_3}}{1 + 2f\alpha_1\alpha_2(1 - \delta_2/2)} \tag{8}$$

where $x_j = \dfrac{2\pi}{\lambda}\sqrt{\epsilon_m}R_j$, $j = 1, 2$, $\gamma_j = 1 - \dfrac{x_j^2}{10}$ and $\delta_j = x_j^2 + \dfrac{2}{3}ix_j^3$. The corrected homogeneous polarizabilities α_j are now explicitly:

$$\begin{aligned}
\alpha_1 &= \frac{\gamma_1(\epsilon - \epsilon_s)}{\epsilon + 2\epsilon_m - \delta_1\gamma_1(\epsilon - \epsilon_s)} \\
\alpha_2 &= \frac{\gamma_2(\epsilon_s - \epsilon_m)}{\epsilon_s + 2\epsilon_m - \delta_2\gamma_2(\epsilon_s - \epsilon_m)} \\
\alpha_3 &= \frac{\gamma_2(\epsilon_m - \epsilon_s)}{\epsilon_m + 2\epsilon_s - \delta_2\gamma_2(\epsilon_m - \epsilon_s)}
\end{aligned} \tag{9}$$

The extinction cross-section is calculated as the sum of absorbance and scattering:

$$C_{\mathrm{ext}}(\lambda) = \pi R_2^2 Q_{\mathrm{ext}}(\lambda) = \pi R_2^2 \left[Q_{\mathrm{abs}}(\lambda) + Q_{\mathrm{sca}}(\lambda)\right] = \pi R_2^2 \left[4x_2 \Im\left(\alpha(\lambda)\right) + \frac{8}{3}x_2^4 \left|\alpha(\lambda)\right|\right] \tag{10}$$

BEM simulations

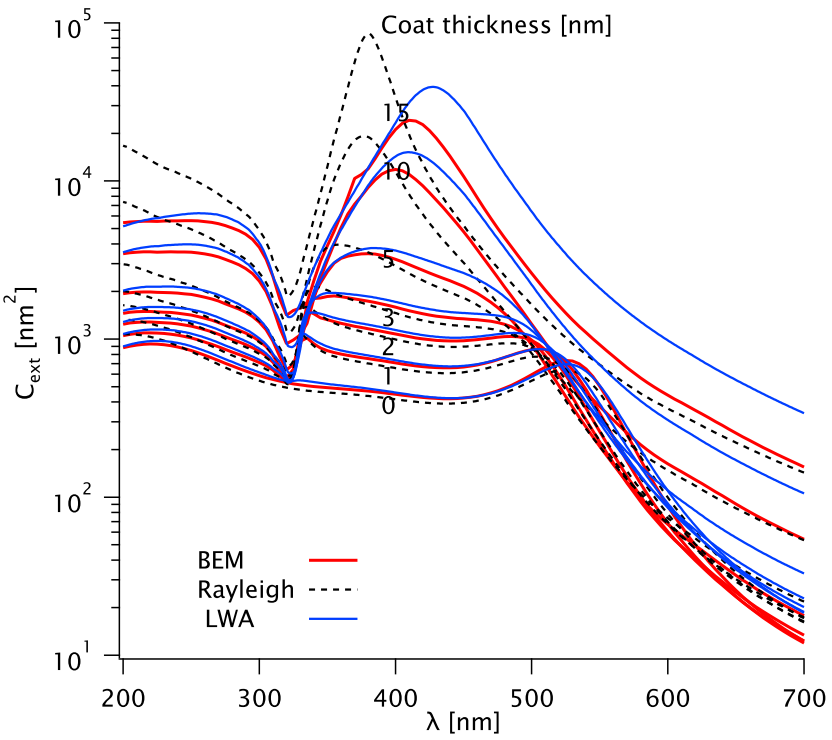

Figure S12: Extinction cross-section simulated using the BEM (red) and calculated in the Rayleigh (black dashes) and LWA (blue) approximations for several shell thicknesses t. Note the logarithmic y scale.

To check the accuracy of (8) we performed BEM simulations, using the MNPBEM toolbox, for core-shell spherical particles with $R_1 = 12.4\,\text{nm}$ and various shell thicknesses $t = R_2 - R_1$. The results are shown in Figure S12. While the Rayleigh approach yields good results for moderate values of t (below about 2 nm), the LWA model is remarkably close to the simulation results for all t values in the wavelength range $200 \leq \lambda \leq 450\,\text{nm}$. For clarity, we do not perform size correction of the dielectric constants, either in the simulations or in the analytical models.

Absorbance spectroscopy fitting

The experimentally measured extinction coefficient $E(\lambda)$ depends on the cross-section (10), but also on the measurement specifics:[S8]

$$E(\lambda) = \frac{n\ell}{\ln 10} C_{\text{ext}}(\lambda) + B \tag{11}$$

where n is the number concentration of particles (in nm^{-3}), ℓ is the optical path length through the solution (in nm) and B is a constant background term. Note that C_{ext} is expressed in nm^2. We use the model (11) to fit the experimental data, as shown in Figure S13. Note that the shape of the fitting curves (with size correction included) is slightly different from the model in Figure (S12).

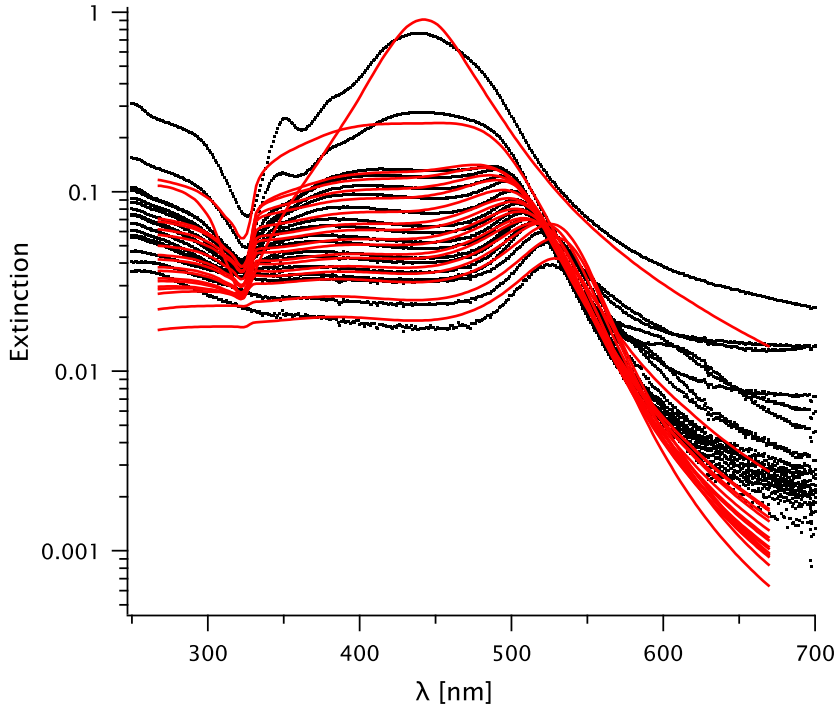

Figure S13: Experimental extinction values (dots) and fits with the model (11) (red lines). The molar Ag/Au ratio K increases from bottom to top.

The fit quality is quite good. As the silver quantity increases, the initial plasmon peak of gold (around 525 nm) flattens and is gradually replaced by a peak around 440 nm char-

acteristic for silver. At the same time, a dip at 320 nm and a peak at 350 nm become more and more marked, due to the interband transitions of silver.

References

(S1) Kline, S. R. Reduction and analysis of SANS and USANS data using IGOR Pro. *Journal of Applied Crystallography* **2006**, *39*, 895–900.

(S2) Johnson, P. B.; Christy, R. W. Optical Constants of the Noble Metals. *Physical Review B* **1972**, *6*, 4370–4379.

(S3) Hövel, H.; Fritz, S.; Hilger, A.; Kreibig, U.; Vollmer, M. Width of cluster plasmon resonances: Bulk dielectric functions and chemical interface damping. *Phys. Rev. B* **1993**, *48*, 18178–18188.

(S4) Bohren, C. F.; Huffman, D. R. *Absorption and Scattering of Light by Small Particles*; Wiley: New York, 1983.

(S5) Meier, M.; Wokaun, A. Enhanced Fields on Large Metal Particles: Dynamic Depolarization. **1983**, *8*, 581–583.

(S6) Chung, H. Y.; Leung, P. T.; Tsai, D. P. Dynamic Modifications of Polarizability for Large Metallic Spheroidal Nanoshells. **2009**, *131*, 124122.

(S7) Chung, H. Y.; Guo, G. Y.; Chiang, H.-P.; Tsai, D. P.; Leung, P. T. Accurate Description of the Optical Response of a Multilayered Spherical System in the Long Wavelength Approximation. **2010**, *82*, 165440.

(S8) Haiss, W.; Thanh, N. T. K.; Aveyard, J.; Fernig, D. G. Determination of Size and Concentration of Gold Nanoparticles from UV-Vis Spectra. **2007**, *79*, 4215–4221.